Hindawi
Advances in Civil Engineering
Volume 2022, Article ID 8357463, 13 pages
https://doi.org/10.1155/2022/8357463

Research Article

Mechanical Characteristics of Variable Cross-Section Immersed Tunnels under Spatial Differential Settlement

Chunshan Yang,[1] **Yatian Wang**,[2] **Lixin Wei**,[1] **and Yizhen Chen**[3]

[1]*Guangzhou Municipal Engineering Design & Research Institute Co., Ltd., Guangzhou, Guangdong 510060, China*
[2]*School of Civil and Traffic Engineering, Guangdong University of Technology, Guangzhou, Guangdong 510006, China*
[3]*School of Civil Engineering, Guangzhou University, Guangzhou, Guangdong 510006, China*

Correspondence should be addressed to Chunshan Yang; soildoctor@163.com

Received 25 May 2022; Accepted 1 July 2022; Published 31 July 2022

Academic Editor: Jian Ji

This work establishes a fine model reflecting the characteristics of immersed tube structures to study the spatial mechanical characteristics of variable cross section immersed tunnels. Then, the mechanical behavior of the pipe segments under differential deformation is explored, based on which we propose a formula for estimating the shear key force and analyze the corresponding failure mechanism and failure mode. Thus, the critical points of the pipe segment design are specified. The results show that, first, the variable cross section segment bears more sectional internal force (over 47%) than the uniform cross section segment in actual cases, which should be fully considered in practical reinforcement design. Bearing deformation alternatively occurs at different shear keys, implying an apparent spatial stiffness matching problem. Second, the pipe segments show overall settlement under longitudinal bending, failing to satisfy the assumption of deformed plane sections. The force on the shear keys varies with the quadratic function of the longitudinal bending degree, and the dislocation magnitude has a positive near-linear relationship with the bending degree. Third, when subjected to torsion, the shear keys of the weak sidewalls are sheared to resist torsion. Then, this force is laterally transferred to the top and bottom plates and jointly shared by the adjacent shear keys, explaining why shear is adjusted with structural deformation. Fourth, under the action of spatial differential deformation, the shear force is mainly undertaken by the vertical shear keys. When the structure is subjected to bending, compression and shear failure occur at the end angle of the middle wall shear key, and its root junction experiences tension and shear failure. When subjected to longitudinal torsion, the local tension and shear failure at the root of the shear key on the soft subgrade side cause a joint failure. Finally, based on the bearing characteristics, failure mechanism, and failure mode of variable cross section immersed tunnels, the idea of strengthening immersed tube structures is put forward, which can guide similar engineers.

1. Introduction

Due to the advantages of a low depth of burial, good stratigraphic applicability, and high section utilization rate, immersed tunnels have been widely used in river- or sea-crossing projects. The fundamental problems existing in their applications have also received more and more attention. Although researchers have conducted relevant studies on pipe segment prefabrication [1], floating and sinking [2], bearing characteristics [3], operation and maintenance [4], and seismic response [5] of immersed tube structures, there are still some shortcomings. The bearing characteristics of immersed tube structures include a segmented body and a joint. In theoretical analysis [6, 7], the limitation is that the conditional setting is too idealistic to comprehensively consider all the influencing factors, while model tests [8, 9] are difficult to conduct, expensive to implement, and limited in the application scope.

In contrast, numerical methods can consider various influencing factors, reflect the actual situation through modeling, have a low cost and sound implementation, and have been more extensively applied. Hu and Xie [10] established a three-dimensional model of immersed pipe segments to simulate the stress and shear distribution

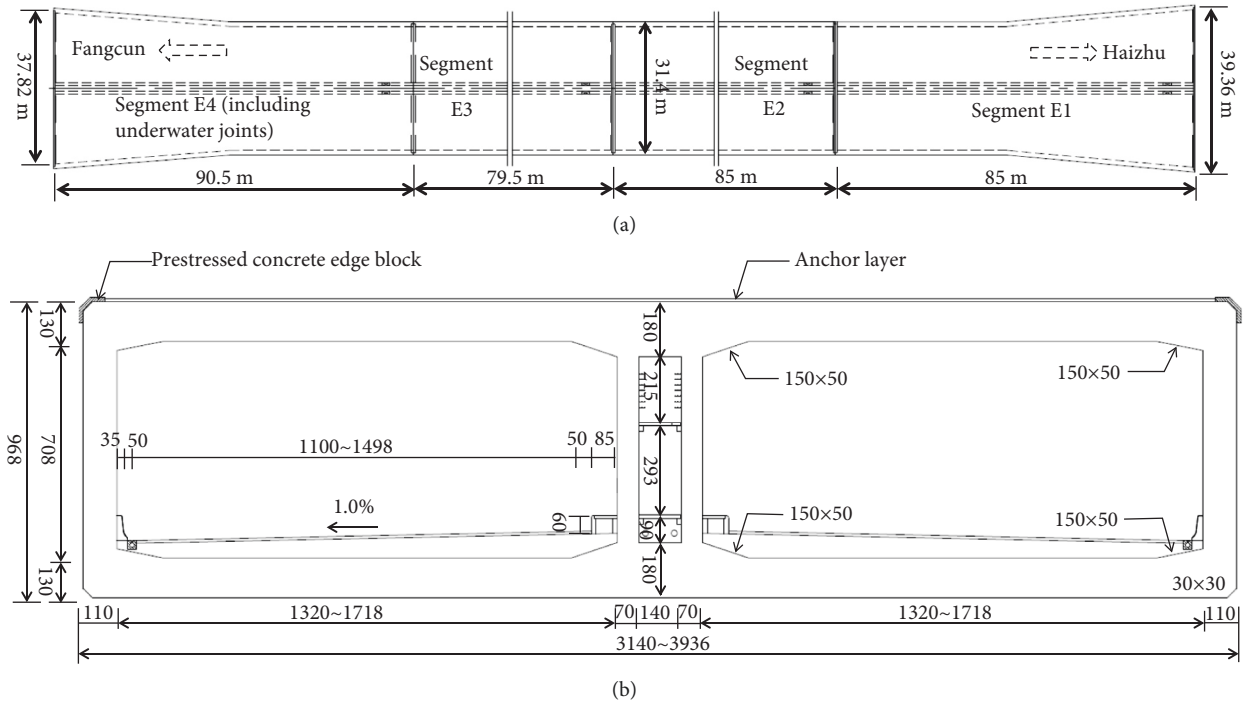

Figure 1: The overall design of the Zhoutouzui tunnel: (a) the tunnel plan; (b) the segment cross section, including the joints.

characteristics of shear keys in the joint of immersed tunnels under the bending and torsion effects; they also described the failure modes of the immersed tunnels. Based on a three-dimensional calculation model, Huang et al. [11] investigated the mechanical properties of tunnel joints under compression-torsion-shear combined conditions and compared them with the properties obtained under the compression-shear combined conditions. Deng et al. [12] also constructed a stratum-structure model and analyzed the effects of the initial stress balance, tunnel settlement deformation, and relative joint deformation.

The existing numerical research primarily focuses on conventional, uniform cross section immersed tunnels. In fact, when the connection between the two sides is limited, the variable cross section segment is often used in immersed tunnels, such as the Zhoutouzui immersed tunnel of Guangzhou city, the Exhibition Center West, and the Shenzhen–Zhongshan Bridge, to fulfill the necessary traffic function requirements. The longitudinal characteristics of the variable cross section immersed tunnels change and their spatial mechanical characteristics are complex. Moreover, the existing research has not explored the internal relationship between the shear key force, joint deformation, and subgrade heterogeneity. Therefore, this paper establishes a numerical model which can reflect the characteristics of immersed tunnel structures, especially the joint deformation, to explore the mechanical properties of the variable cross section segment subjected to spatial differential deformation. Furthermore, we develop a formula for estimating the shear key force, analyze the failure mechanism and failure mode of variable cross section immersed tunnels, and propose the critical points of pipe segment design.

2. Engineering Case

The Zhoutouzui immersed tunnel of Guangzhou city crosses the Pearl River, where the Hualei Road of Fangcun and Hongde Road Flyover of Haizhu District inner ring road lie on its west and east sides. The tunnel traversing 340 m of the Pearl River section is divided into segments E1, E2, E3, and E4 by the immersed tube method (Figure 1). The reserved distance between the overpass and the immersed tunnel ends is short, and the elevation is high. Pipe segments E1 and E4, connecting the immersed tunnel and the open-cut tunnel on the shore, adopt variable cross section segments to maintain good driving conditions and satisfy the requirements of connection deceleration and gradient section standards. Table 1 lists the physicomechanical parameters of the soil and the structure. The corresponding strength of the reinforced concrete structure is also calculated based on the deformation coordination [13].

3. Simulation Development and Verification

3.1. Analytical Model and Working Conditions. Since the dead weight of the immersed pipe is less than that of the excavated soil, the subgrade of the pipe segment can be regarded in the elastic state, and the subgrade spring can simulate the subgrade effect on the structure. According to the displacement characteristics of the pipe structure, the radial spring of the compression side is set. As shown in Figure 2, the stress area method is adopted to calculate the distribution of the coefficient of the subgrade reaction based on the soil parameters listed in Table 1 [14].

Table 1: The physicomechanical parameters of the soil and the structure.

Soil type	Density, ρ ($g{\cdot}cm^{-3}$)	Consolidated quick shear Cohesion, c (kPa)	Consolidated quick shear Internal friction angle, φ (°)	Compression modulus (MPa)	Poisson's ratio
Fill	1.80	7.80	8.20	2.51	0.32
Silty fine sand	1.76	2.00	20.0	2.49	0.28
Plastic loam	1.95	33.2	16.2	4.10	0.33
Hard plastic loam	1.96	38.0	17.1	5.76	0.30
Completely weathered rock	2.07	42.1	22.3	14.8	0.25
Strongly weathered rock	2.10	55.2	26.1	25.0	0.24
Mildly weathered rock	2.50	200	28.0	80.0	0.30
Weakly weathered rock	2.60	500	30.0	150	0.29
Structure type	**Density, ρ ($g{\cdot}cm^{-3}$)**	**Cohesion, c (kPa)**	**Internal friction angle, φ (°)**	**Elastic modulus (MPa)**	**Poisson's ratio**
Segment C40	2.43	5000	58	32500	0.167
Reinforcement	7.85	210000	0	200000	0.2
Reinforced concrete	2.5	5265	59.3	—	—
Rubber bearing	0.93	—	—	250–12500	0.499

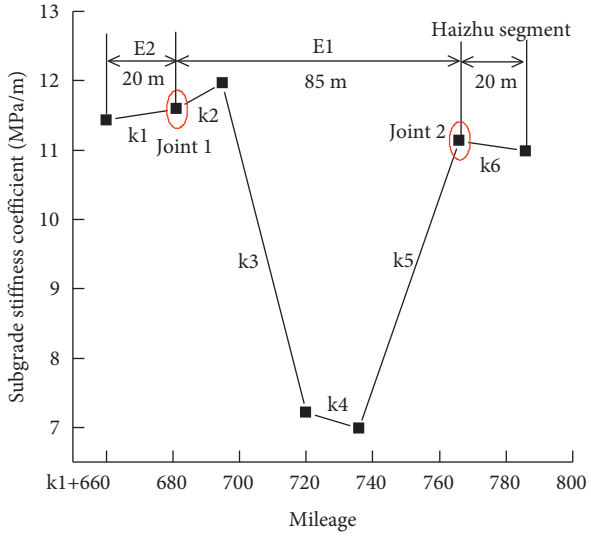

Figure 2: The subgrade stiffness coefficient.

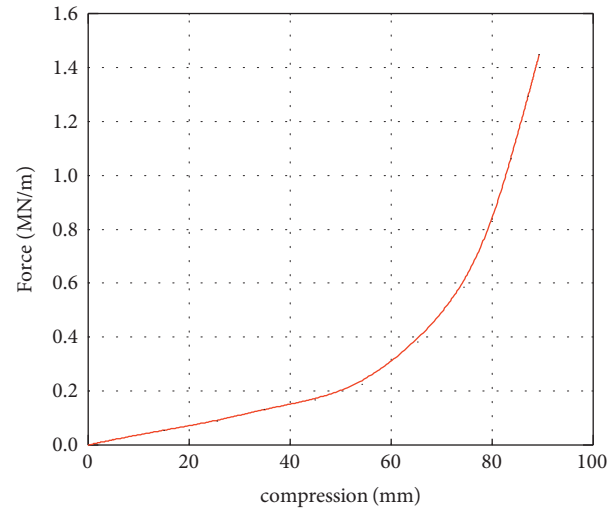

Figure 3: The load–displacement relationship of the GINA waterstop.

The model considers all the pipe segments, joints, connectors, and joint gaps to be three-dimensional solid elements, and a fine calculation model is established according to the actual situation. Pipe segments and shear keys are elastoplastic constitutive models, following the Mohr–Coulomb yield criterion, and connectors and joint gaps are elastic constitutive models. The rubber bearing is subjected to elastic deformation and soon becomes rigid. Its initial elastic modulus is 250 MPa, and the modulus after hardening is 12500 MPa, adopting the compression double-line spring element. The GINA waterstop also uses nonlinear spring elements, the forced-induced deformation of which is shown in Figure 3.

Since there is no internal force on the solid element, it is impossible to observe the internal force in the pipe segment visually. Therefore, the typical section of segment E1 is equipped with low-stiffness beam elements for internal force testing, which is based on deformation coordination and uses deflection curve equation for conversion. Figure 4 illustrates the overall and detailed models of the segment joints.

The load combination of the calculation model comprises 1.35 times the structure weight, 1.35 times the payload weight, 1.35 times the soil overburden weight, 1.35 times the buoyancy, 1.35 times the lateral Earth pressure, the temperature load, and 1.08 times the traffic load. Based on the corresponding model under actual engineering geological conditions, the force-induced deformation characteristics of the immersed tunnel caused by the heterogeneity of the internal and external pipe segments (bending and torsion) are abstractly characterized by changing the coefficient of the

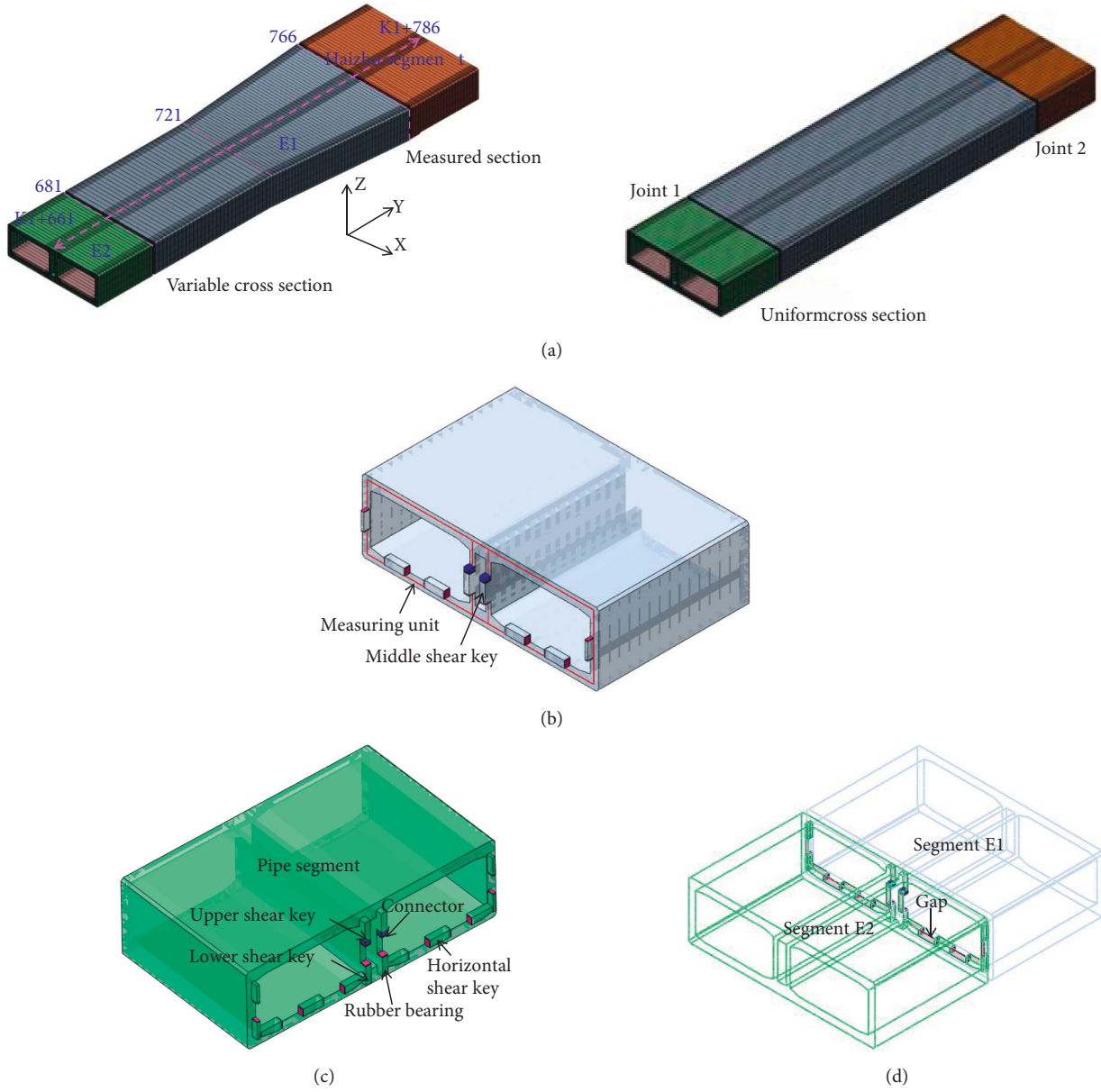

Figure 4: The three-dimensional calculation model: (a) the overall model; (b) the detailed model of the joint of segment E1; (c) the detailed model of the joint of segment E2; (d) the connection model of segments E1 and E2 with a local display of segment E1.

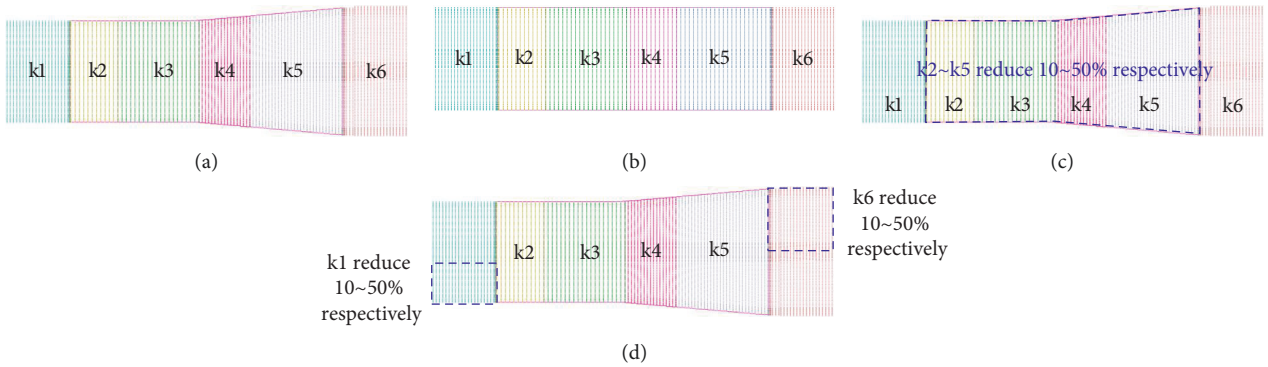

Figure 5: The diagram of (a) working condition 1 with a variable cross section, (b) working condition 2 with a uniform cross section, (c) working conditions 3–7, and (d) working conditions 8–12.

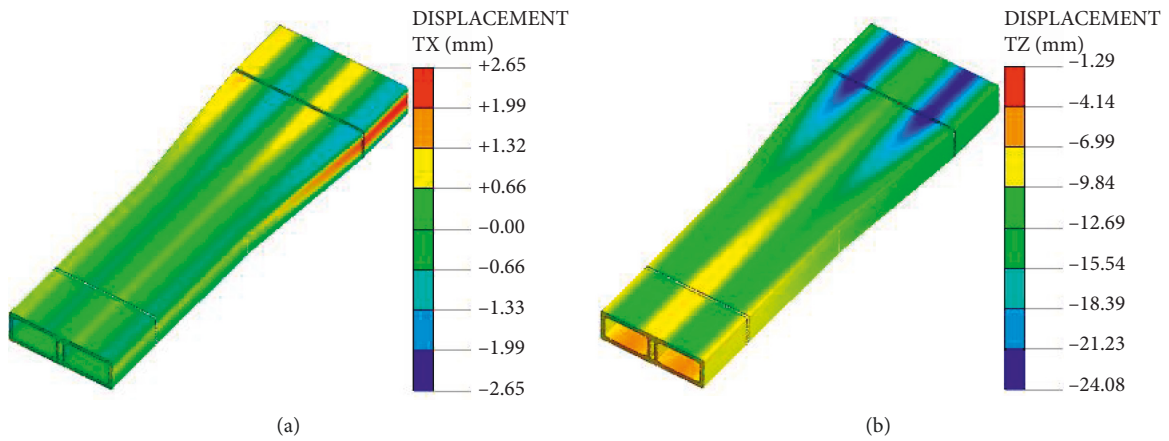

Figure 6: The displacement nephogram under working condition 1: (a) horizontal displacement; (b) vertical displacement.

subgrade reaction. Figure 5 depicts the related detailed working conditions.

3.2. Validating Model Rationality. Figure 6 depicts the displacement nephogram under working condition 1. The displacement is positive when it points to the coordinate in a positive direction and negative when it points to the coordinate in a negative direction. The most apparent displacement areas under working condition 1 appear in the variable cross section of segment E1 and the Haizhu segment. The maximum horizontal and vertical displacements are 2.65 and 24.08 mm, respectively. The displacement is manifested as the subsidence of the long-span roof under a vertical load and the sidewall arch accompanied by settlement.

After the completion of construction, 83 monitoring points (measured sections) were laid along the tunnel during the operation of the project. Laser section meters monitored the convergence displacement of the tunnel section. The calculated results of the monitoring points in Figure 7 are compared with the measured data, as shown in Figure 8, to verify the reliability of the calculation model.

According to the displacement comparison results in Figure 8, the calculated data reflect the actual deformation trend of the immersed tunnels, indicating that the calculation model is rational to some extent. However, the maximum difference between the calculated and measured results is about 12%, with an average difference of 0.45 mm, which is primarily caused by the subgrade effect on the structure and the difference in the selected soil parameters used in the calculating process.

4. Spatial Mechanical Characteristics of Variable Cross-Section Segment

4.1. Contrastive Analysis of Force on Variable and Uniform Cross Sections. Summarizing Figures 9–11 provides the force-induced deformation results of the Haizhu segment and joint 2, as listed in Table 2. Table 2 demonstrates that the maximum bending moment of the variable cross section segment is 2041.1 kN·m, 32.19% higher than that of the

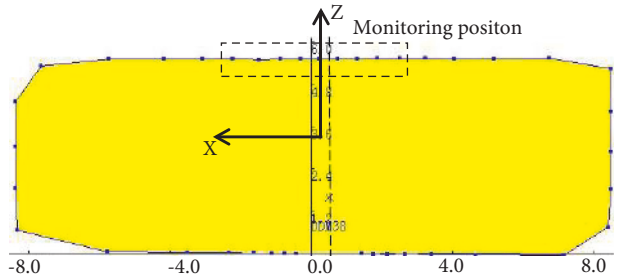

Figure 7: The layout of the monitoring points.

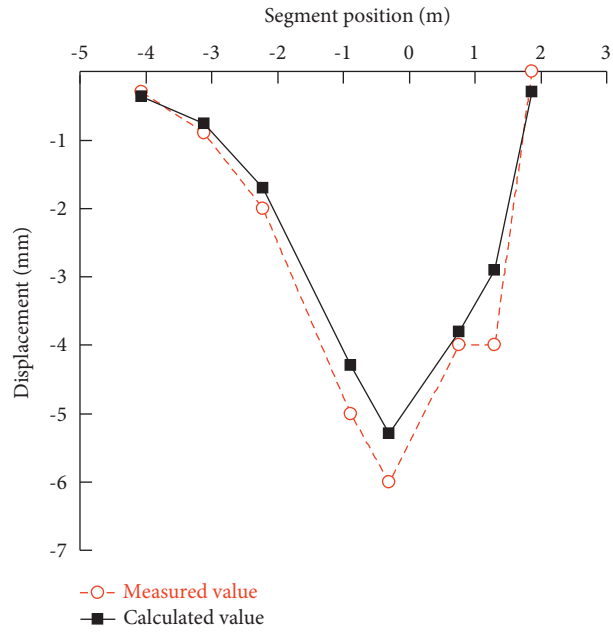

Figure 8: Comparing the calculated results with the measured data.

uniform cross section segment, 1384.1 kN·m, which is due to the larger span of the variable cross section segment under the same loading conditions.

In the variable cross section segment, the maximum shear value of the joint shear key is 3451.16 kN, which occurs

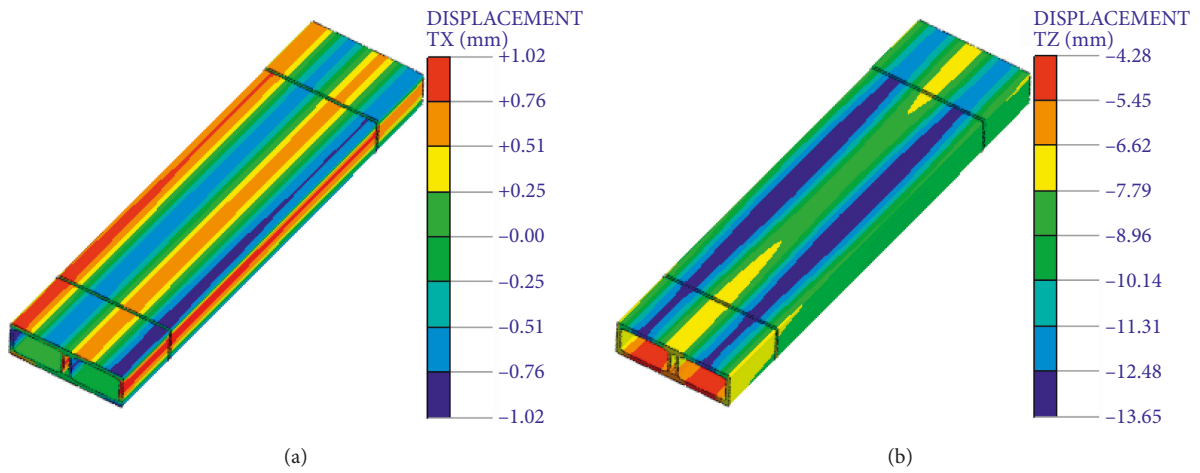

Figure 9: The displacement nephogram under working condition 2: (a) horizontal displacement; (b) vertical displacement.

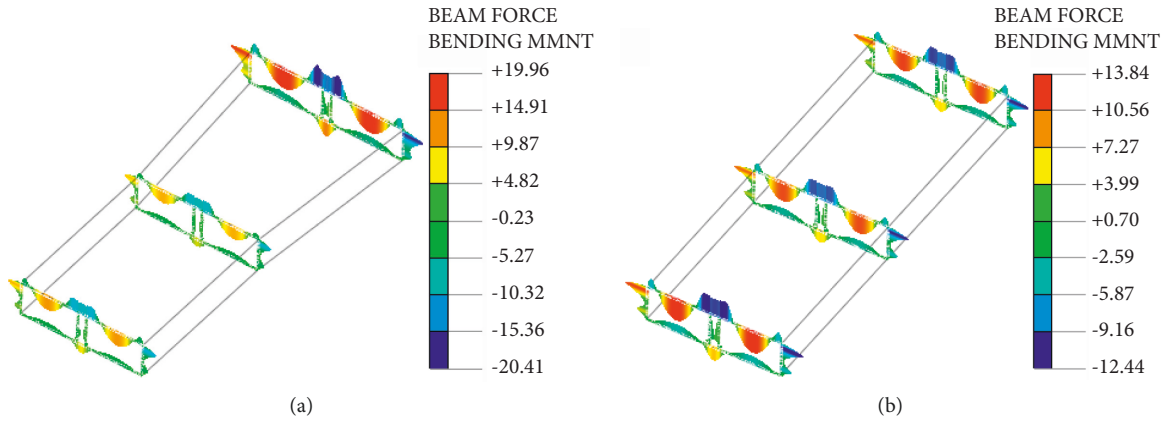

Figure 10: The bending moment nephogram of segment E1 with a (a) variable cross section and (b) uniform cross section (×100 kN·m).

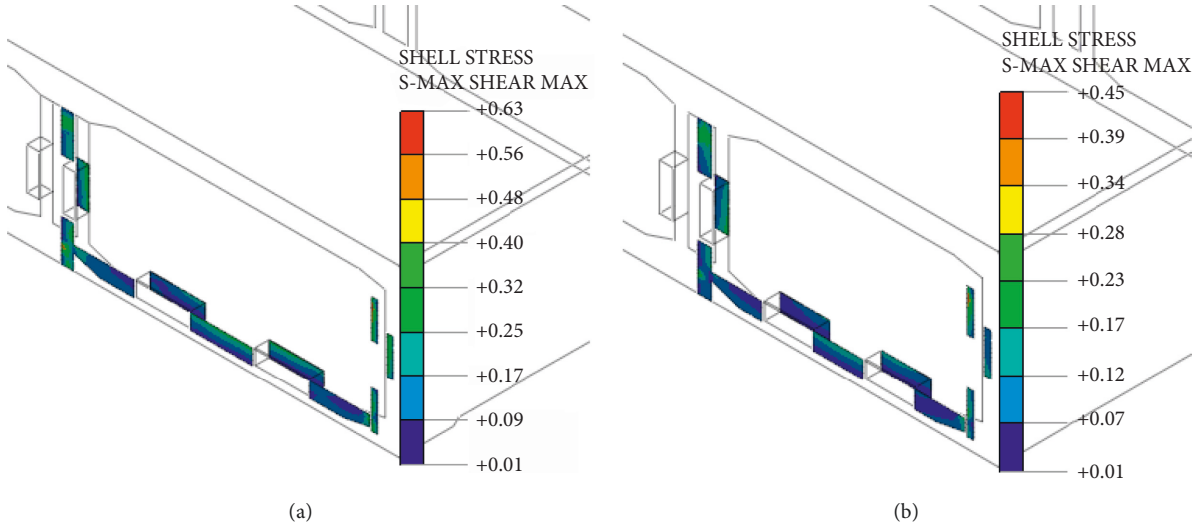

Figure 11: The shear stress nephogram of joint 2 with a (a) variable cross section and (b) uniform cross section (kPa).

Table 2: The force-induced deformation of the Haizhu segment and joint 2.

Cross section type	Maximum bending moment (kN·m)	Vertical shear force on the middle wall (kN)	Vertical shear force on the sidewall (kN)	Maximum horizontal displacement (mm)
Uniform	1383.94	2120.20	885.57	1.02
Variable	2041.10	3451.16	2106.45	2.65
Difference value (%)	47.48	62.78	137.86	159.8
Maximum vertical displacement (mm)	Opening magnitude (mm)	Compression magnitude (mm)	Dislocation magnitude (mm)	
13.65	0.29	0.13	0.20	
24.08	0.20	0.24	0.23	
76.41	–31.03	84.62	15.0	

on the middle wall and is lower than the 5060 kN shear design value, fulfilling the bearing requirements. The ratio of the shear bearing of the sidewall to that of the middle wall of the variable cross section segment is 0.19 : 0.31 : 0.31 : 0.19. However, the ratio of the shear bearing of the sidewall to that of the middle wall of the uniform cross section segment is 0.15 : 0.35 : 0.35 : 0.15. There is a slight difference between the two schemes because the lateral dimension of the variable cross section segment is large, its spatial effect is noticeable, and the contribution of the sidewall is increased. It is also found that the forces and deformations of each shear key in space restrict and influence each other. However, in real cases, the stiffness of the middle wall shear key is higher, and the shear deformation of the sidewall develops faster under an external load. The stress is redistributed after reaching a specific value, and the middle wall bears more loads and produces shear deformation. With the shear deformation development of the middle wall shear key, the stress is adjusted for the second time, and the load on the sidewall increases gradually. This series of actions is repeated until the structure is damaged or destroyed, so there is a problem with spatial stiffness matching between the shear keys.

In terms of stress-induced deformation, the variable cross section segment has a significantly larger internal force and deformation than the uniform cross section segment, which should be fully considered in practical engineering. In addition to satisfying the requirements of load-bearing and deformation, the variable cross section segment can be used for the smooth connection of road networks.

4.2. Mechanical Bending Characteristics of Variable Cross-Section Segment. The immersed tunnel is mainly subjected to bending and torsion, including the longitudinal bending induced by vertical strata heterogeneity, different external actions, and characteristic structural differences and the longitudinal torsion induced by horizontal strata heterogeneity and effect differences. Working conditions 3–7 in Figure 5(c) correspond to the longitudinal bending of different degrees. Figures 12 and 13 depict the calculated settlement nephogram under working condition 7 and the calculated settlement increment curve under different working conditions, respectively.

Comparing the settlement results under working conditions 1 and 7 demonstrates that the subgrade stiffness coefficient in segment E1 declines by 50%; that is, its longitudinal heterogeneity increases. The maximum settlement of the variable cross section segment only increases by 12.7%. Moreover, the reduction of the subgrade stiffness coefficient does not cause a remarkable deformation of the segment body, and segment E1 is primarily in the overall vertical settlement. In terms of deformation, segment E1 under working conditions 3–7 has a profound effect near segment E2. Therefore, the mechanical properties of joint 1 are mainly explored.

Figure 14 delineates the displacement of joint 1 under different working conditions. The displacement is negative when opening upward and positive when opening downward. It can be concluded from Figure 14 that, first, there is a positive near-linear relationship between the joint dislocation magnitude and the subgrade heterogeneity. The reduction of the subgrade stiffness coefficient increases the dislocation of the pipe segments, with a maximum dislocation of 0.428 mm, which is smaller than the control value. Second, due to the deformation of the segment structure itself, the assumption of deformed plane sections cannot be satisfied. The distributions of compression and opening magnitude are different, and the latter is on average 35.39% larger than the former. Third, with the reduction of the subgrade stiffness coefficient, in the vertical direction of the segment, the pattern of stress on joint 1 changes from "upper tension, lower compression" to "upper compression, lower tension," with a maximum open magnitude of 0.428 mm and maximum compression of 0.577 mm.

Figure 15 plots the settlement increment and the dislocation magnitude of the pipe segment in the same graph to reveal the internal relationship between the settlement caused by the bending of the variable cross section segment and the joint dislocation magnitude. Thus, (1) expresses the correlation between the settlement increment ($\triangle S$) and the dislocation magnitude (δ):

$$\Delta S = 11.05\delta^2 + 3.82\delta - 0.152. \quad (1)$$

Figure 16 depicts the bending moment of segment E1 under working condition 7. Its maximum bending moment is 2046.4 kN·m, which is close to the bending moment under working condition 1. The longitudinal bending degree slightly affects the internal force on the

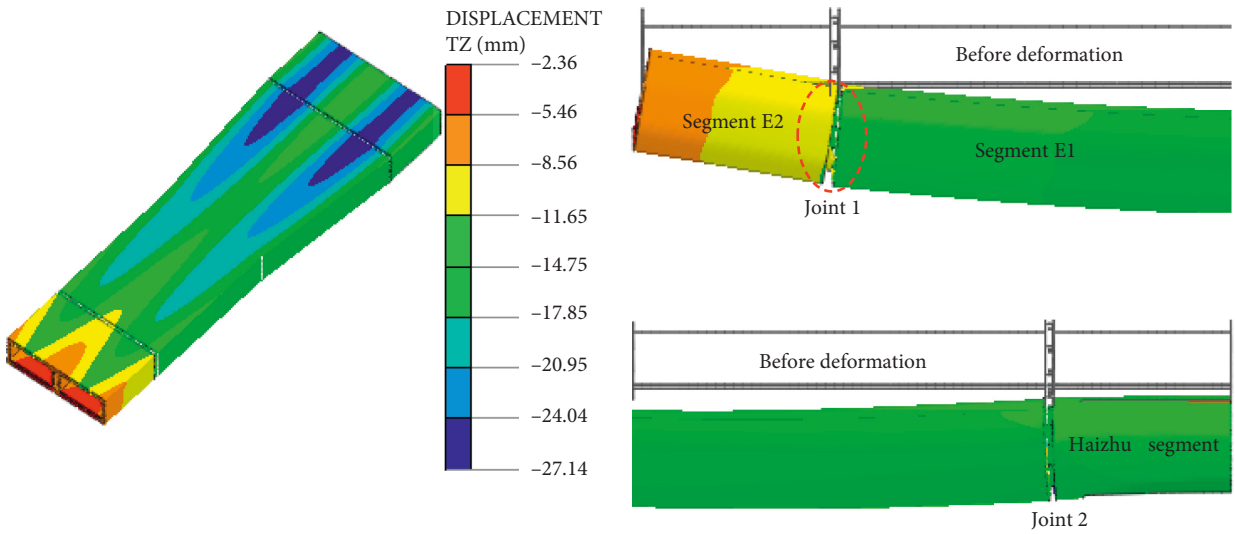

Figure 12: The vertical displacement and deformation under working condition 7: (a) settlement nephogram; (b) spatial deformation at a ×2 magnification.

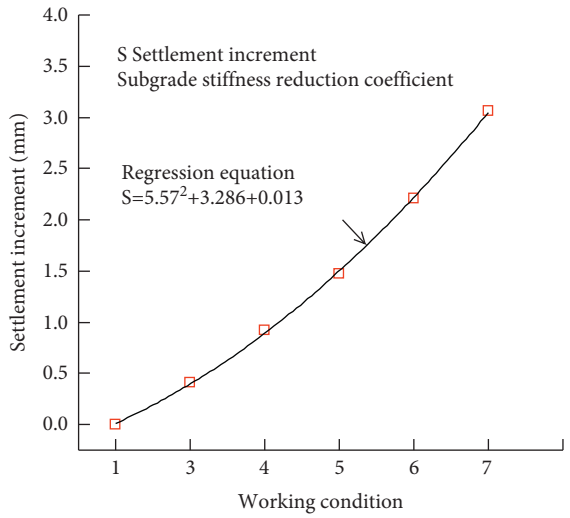

Figure 13: The settlement increment under different working conditions.

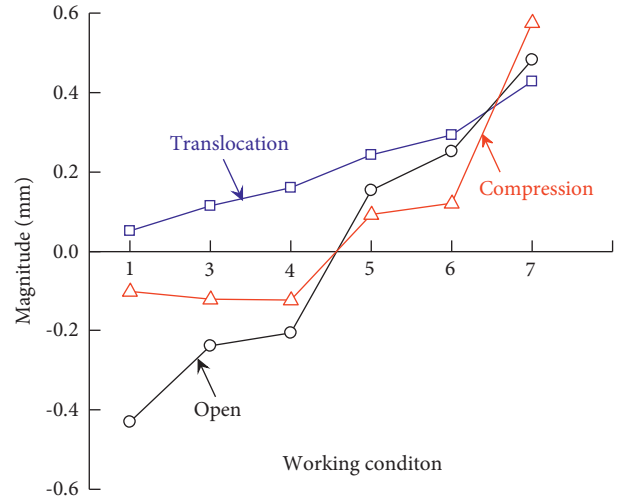

Figure 14: The displacement of joint 1 under different working conditions.

pipe segment, which further indicates that enhancing the longitudinal heterogeneity influences the horizontal deformation of the pipe segment negligibly, and it is in overall settlement.

Figure 17 shows the nephogram of the shear stress on joint 1 under different working conditions. The shear force on joint 1 under different working conditions is determined by integration, as presented in Figure 18. The shear stress on the shear keys enlarges gradually with an increase in longitudinal heterogeneity, and the joint mainly resists the shear force by the vertical shear key when the segment is bent longitudinally. The maximum shear on the middle wall shear key and the sidewall shear key is 3925.29 and 1412.94 kN, respectively. The shear-bearing ratio is 0.14 : 0.36 : 0.36 : 0.14, which is close to that of joint 1. The dislocation magnitude and shear force (Q) satisfy the following relationship:

$$Q = 10738.8\delta^2 - 420.43 + 2404\delta.36. \quad (2)$$

The actual project is based on the completion of tunnel construction, and the measured settlement value after the operation is the settlement increment. Equations (1) and (2) estimate the dislocation magnitude and shear key force of the immersed tunnel joint, respectively; otherwise, the elastic foundation beam theory can calculate the settlement values under different loads to estimate these two values.

4.3. Mechanical Torsion Characteristics of Variable Cross-Section Segment. Figure 19 shows the displacement nephogram of segment E1 under working condition 12. The difference in the structural displacement, especially the vertical displacement, of segment E1 and the Haizhu

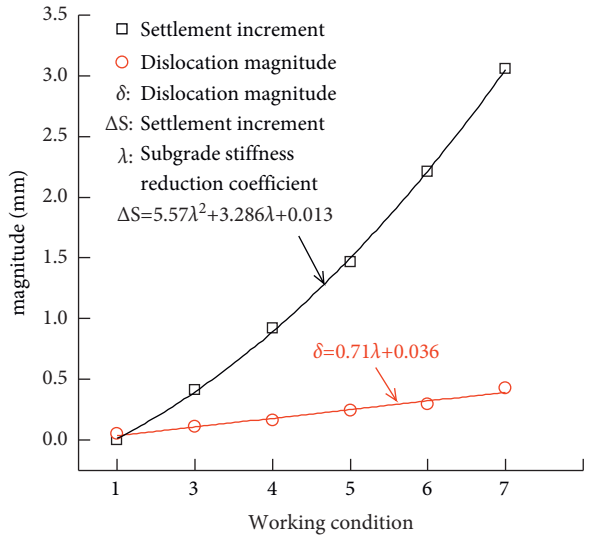

Figure 15: The relationship between the settlement increment and the dislocation magnitude.

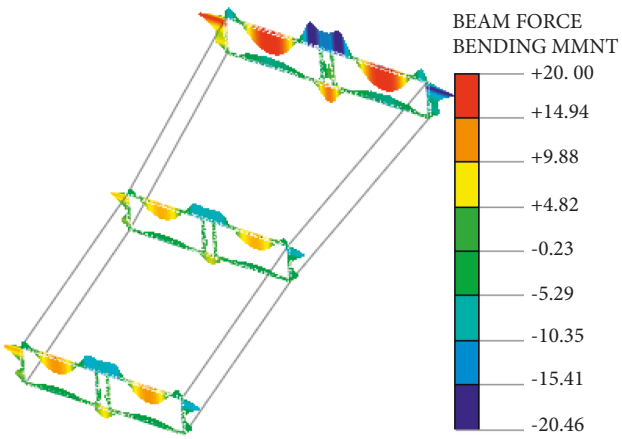

Figure 16: The bending moment of segment E1 under working condition 7 (×100 kN·m).

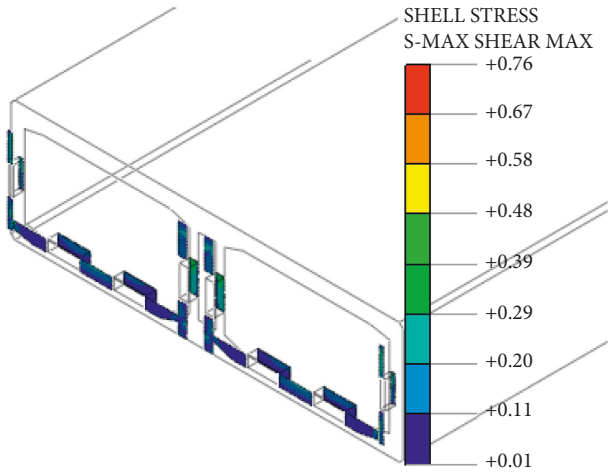

Figure 17: The nephogram of the shear stress on joint 1 under different working conditions.

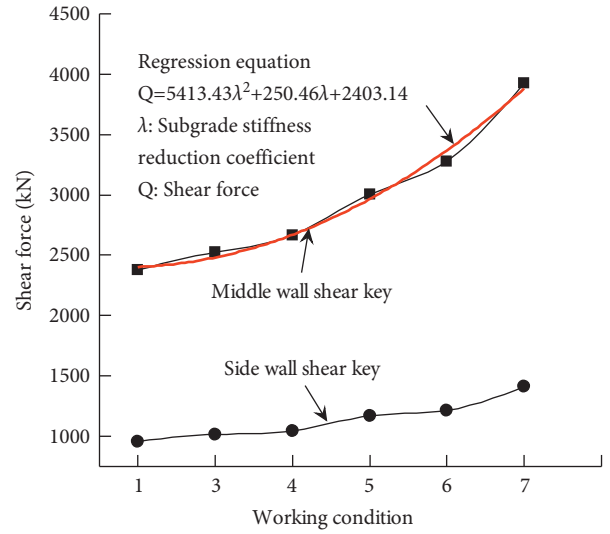

Figure 18: The shear force on joint 1 under different working conditions.

segment in the variable cross section tunnel is relatively noticeable. Therefore, the vertical displacement of the measured section (Figure 4(a)) under different working conditions is extracted to plot Figure 20.

Figure 20 demonstrates that the difference in the displacement of the symmetrical position on both sides of the segment top and bottom plates enlarges with an increase in the subgrade heterogeneity; that is, torsion affects the pipe segment more and more. Working condition 12 corresponds to a reduction of the subgrade stiffness coefficient by 50%, and the maximum difference in the displacements of the left and right walls of the segment is 2.19 mm. Figure 21 shows that the Haizhu segment and segment E1 are in relative dislocation under torsional conditions, and the dislocation magnitude enlarges linearly with an increase in the subgrade stiffness reduction coefficient (λ) as follows:

$$\delta = 0.686\lambda + 0.2. \tag{3}$$

Figure 22 depicts the bending moment of segment E1 under torsion condition 12. The buried section of the Haizhu segment and the uneven horizontal settlement of immersed segment E2 cause the longitudinal torsion of the segment. However, the torsion is primarily resisted by the joints between the segments, and the segment body has no obvious deformation. It has almost no influence on the bending moment of segment E1, the maximum bending moment of which is 2090.5 kN·m.

Figure 23 shows the nephogram of the shear stress on joint 2 under working condition 12. The vertical shear key still bears the longitudinal torsion shear of the segment, and the shear force under different working conditions is obtained by conversion, as presented in Figure 24.

The settlement of the buried section of the Haizhu segment occurs first on the side with reduced subgrade stiffness, and this sidewall shear key is sheared to resist the torsion. Then, this force is laterally transferred to the top and bottom plates and jointly shared by the adjacent shear keys. Its essence is constantly adjusting the shear of the shear key

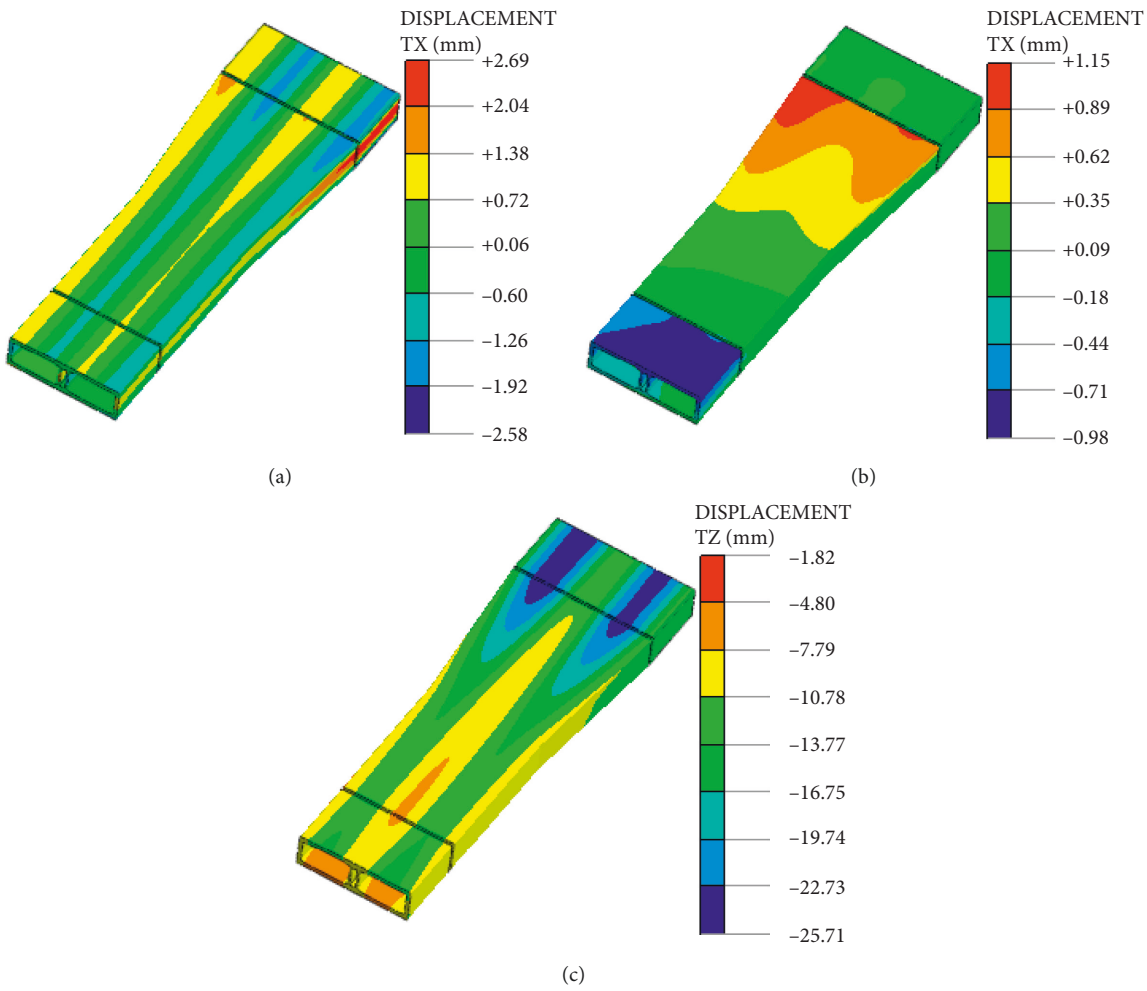

Figure 19: The nephogram of the displacement of segment E1 under working condition 12: (a) x-direction; (b) y-direction; (c) z-direction.

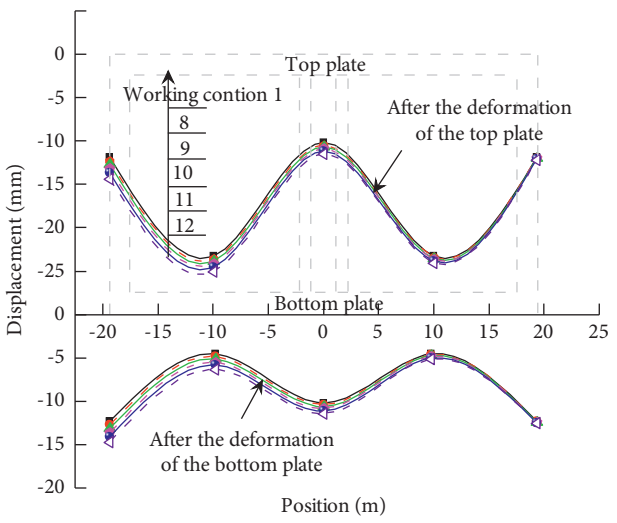

Figure 20: The settlement of the monitored section under torsion.

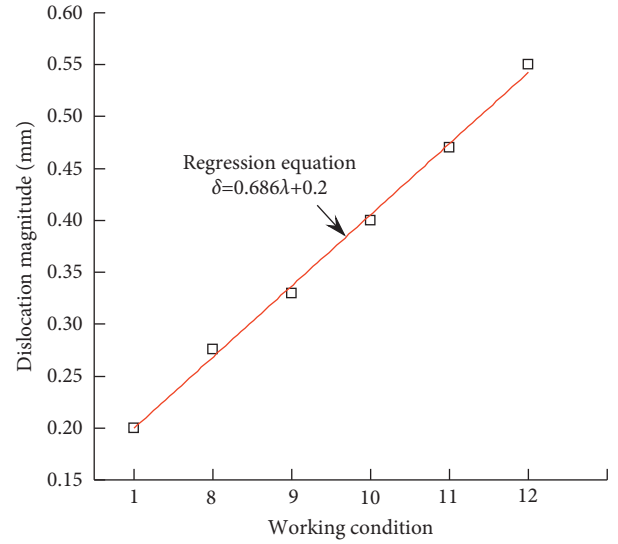

Figure 21: The dislocation magnitude under different torsion conditions.

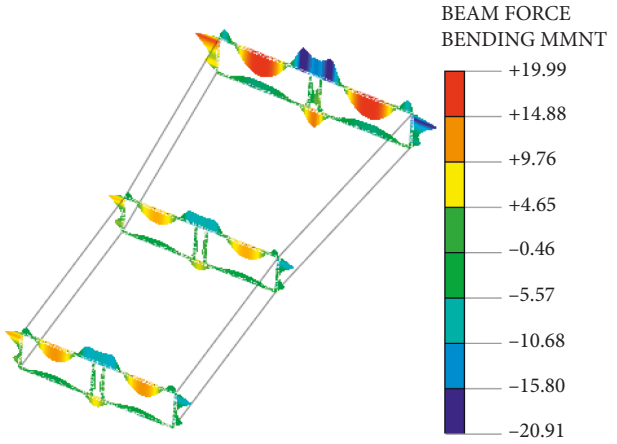

Figure 22: The bending moment of segment E1 under torsion condition 12 (×100 kN·m).

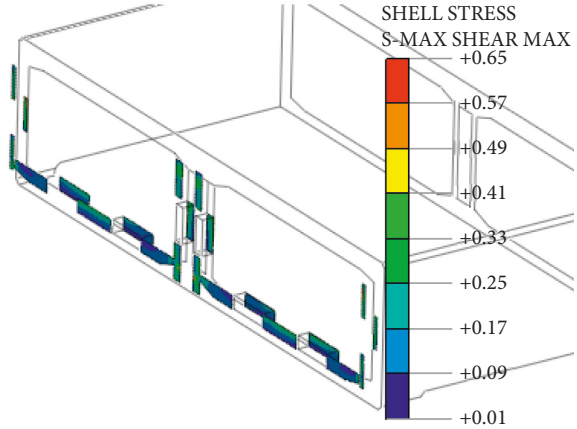

Figure 23: The nephogram of the shear stress on joint 2 under working condition 12.

with the structural displacement and shear key deformation. Figure 24 demonstrates that the shear of each shear key enlarges nearly linearly with an increase in the segment torsion degree and the maximum shear force still appears on the middle wall. However, the shear slope of the left wall is the largest, with a maximum increment of 320 kN, because the subgrade stiffness is reduced therein.

It should be noted that the torsional shear force on the sidewall plays a leading role in the experiments reported in [15, 16]. The first reason is that there are differences in the pipe segment structure of the two. Secondly, [15, 16] achieved longitudinal torsion through considerable forced displacement, resulting in the apparent compression of shear keys on the sidewalls. In fact, in this case, the shear key force varies at a higher rate with the torsion degree on the sidewall than on the middle wall. When the torsion degree is large enough, the shear force will be greater on the sidewall shear key than on the middle wall shear key, similar to the situation reported in [15, 16].

In addition, based on the relationship between the maximum shear force on the joint, the dislocation

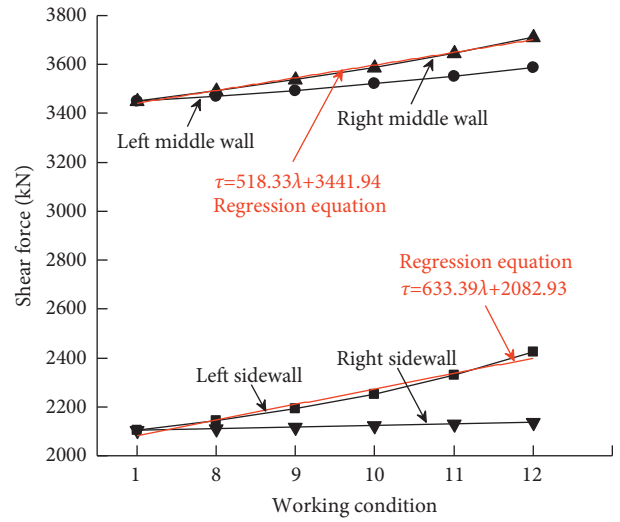

Figure 24: The shear force on joint 2 under different working conditions.

magnitude, and the subgrade stiffness reduction coefficient, the correlation between the dislocation magnitude and the maximum shear force on the middle wall (τ) is defined as follows:

$$\delta = 0.686\lambda + 0.2. \quad (4)$$

5. Damage and Failure Mechanism of Tunnel and Design Key Points

Utilizing variable cross section segments affects the spatial transmission and load-bearing characteristics of segmental structures but does not change the damage to and failure mode of such structures. Immersed tunnels do not collapse as a whole, and damage and failure occur at the relatively weak and sensitive joints. Immersed pipe joints mainly experience the processes of (1) the elastic deformation of the rubber bearing, (2) the joint bearing of the rubber bearing and shear key, (3) the plastic deformation of the shear key, and (4) the damage to and failure of the shear key in sequence [17]. The joint shear key causes structural failure, so the stress on the joint shear key should be investigated. Figure 25 displays the nephogram of the stress on the shear key.

From the stress distribution law of the shear keys, it can be deduced that the stress concentration occurs at the bottom end angle of the middle wall shear key and at the junction between the lower shear key and the pipe segment of the middle wall and the sidewall. When the structure is subjected to bending, compression and shear failure occur at the end angle of the middle wall shear key, and its root junction experiences tension and shear failure. When the segment is under longitudinal torsion, the joint failure occurs at the junction between the middle wall shear key and the segment on the side of the soft subgrade. It is a local tension and shear failure.

Given the failure mechanism of immersed tunnels, the key to the tunnel structure design lies in using accurate

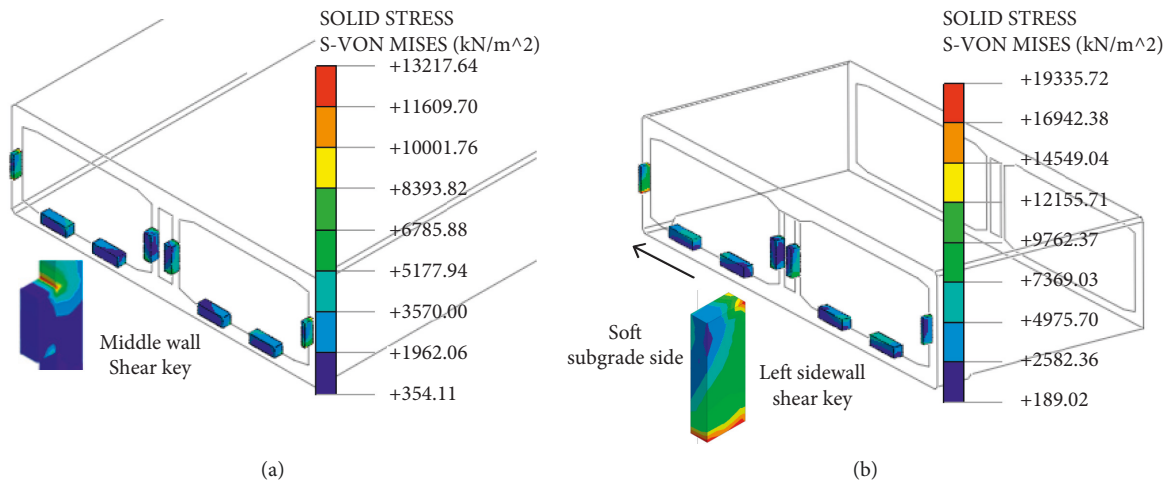

Figure 25: The von Mises stress nephogram of the shear key of (a) joint 1 on segment E1 under working condition 7 and (b) joint 2 on the Haizhu segment under working condition 12.

identification methods[18] and formulating effective prevention and control measures for standard joint failure modes. The shear key end angle, joint, and pipe segment connection should be optimized and strengthened. For example, the local compressive stress can be reduced by changing the shape of the shear key locally to avoid the compression-shear failure of the shear key caused by the stress concentration at the end angle. Alternatively, embedded parts, memory bearing [19], and tensile reinforcement bars at the junction of the shear key and the pipe segment can be added to avoid the cracking of the shear key at this position. Meanwhile, on the basis of the deformation characteristics of the variable cross section segment, various reinforcement schemes should be made for different positions of the segment.

6. Conclusions

By utilizing a numerical method, we established a fine three-dimensional finite model of immersed tunnels. The mechanical characteristics of the variable cross section segment under spatial differential deformation were also analyzed in depth. We proposed a formula for estimating the shear key force and analyzed the corresponding failure mechanism and failure mode. The following main conclusions can be drawn from the findings of this work:

(1) The shear keys with different stiffness are subjected to alternate load deformation and stress adjustment until the structure is damaged or destroyed, so there is a problem in matching the spatial stiffness of the shear keys. In actual cases, under similar conditions, the variable cross section segment bears more sectional internal force (over 47%), and its deformation is larger than the uniform cross section segment. In addition to fulfilling the requirements of load-bearing and deformation, the variable cross section segment can be used for the smooth connection of road networks.

(2) The longitudinal bending slightly affects the horizontal deformation of the segment. The pipe segments show overall settlement under longitudinal bending, failing to satisfy the assumption of deformed plane sections. The shear of the shear key enlarges gradually with an increase in longitudinal heterogeneity. The joint mainly resists the shear force by the vertical shear keys, and there is a positive near-linear relationship between the joint dislocation magnitude and the longitudinal heterogeneity.

(3) The joints between the segments mainly resist the torsion, and the segment body has slight deformation. Further, the shear force is borne by the vertical shear key, and the sidewall shear key is sheared to resist the torsion. Then, this force is laterally transferred to the top and bottom plates and jointly shared by the adjacent shear keys.

(4) When the structure is subjected to bending, compression and shear failure occur at the end angle of the middle wall shear key, and its root junction experiences tension and shear failure. When the segment is under longitudinal torsion, the joint failure happens at the root of the shear keys in the soft subgrade. It is a local tension and shear failure.

(5) Based on the failure mechanism of immersed tunnels, the key to the tunnel structure design is to formulate effective prevention and control measures for standard joint failure modes. The shear key end angle, joint, and pipe segment connection should be optimized and strengthened.

The quantitative relationship between the joint displacement, the shear key force, and the subgrade stiffness coefficient is primarily based on the analysis of actual cases in this paper. However, its applicability still needs further demonstration. Thus, in the follow-up work, our team will perform further analyses based on the new project of variable cross section immersed tunnels to obtain more scientific and reasonable results.

Data Availability

Some or all data, models, and code that support the findings of this study are available from the corresponding author.

Conflicts of Interest

The authors declare that they have no conflicts of interest.

Acknowledgments

This project was supported by the National Natural Science Foundation of China (51508119) and the Natural Science Foundation of Guangdong Province (2020A1515011058).

References

[1] X. Liu, W. Jiang, G. D. Schutter, Y. Yuan, and Q. Su, "Early age behavior of precast concrete immersed tunnel based on degree of hydration concept," *Structural Concrete*, vol. 15, no. 1, pp. 66–80, 2014.

[2] Z. Y. Xiong, C. S. Yang, and L. W. Chen, "Hydrodynamic characters and program evaluation of immersed tunnel with variable section during floating and sinking process," *Journal of Hefei University of Technolgy (Natural Science)*, vol. 43, no. 1, pp. 88–93, 2020.

[3] B. Y. Fu and S. Y. Song, "Analysis of immersed tunnel settlement under complex load and multiple kinds of compound foundations," *IOP Conference Series: Earth and Environmental Science*, vol. 787, no. 1, Article ID 012191, 2021.

[4] M. J. Wu, Q. Zhang, and S. Y. Wu, "Risk assessment of operation period structural stability for long and large immersed tube tunnel," *Procedia Engineering*, vol. 166, pp. 266–278, 2016.

[5] K. Zhao, S. D. Zhu, X. X. Bai et al., "Seismic response of immersed tunnel in liquefiable seabed considering ocean environmental loads," *Tunnelling and Underground Space Technology*, vol. 115, Article ID 104066, 2021.

[6] W. H. Xiao, H. T. Yu, Y. Yuan, L. Taerwe, and G. Xu, "Compression-shear behavior of a scaled immersion joint with steel shear keys," *Tunnelling and Underground Space Technology*, vol. 70, pp. 76–88, 2017.

[7] H. T. Yu, Y. Yuan, H. Z. Liu, and L Z xin, "Mechanical modeland analytical solution for stiffnessin the joints of an immersed tube tunnel," *Engineering Mechanics*, vol. 31, no. 6, pp. 145–150, 2014.

[8] J. Q. Lin, Y. L. Dong, J. T. Duan, D. Zhang, and W. Zheng, "Experiment on single-tunnel fire in concrete immersed tunnels," *Tunnelling and Underground Space Technology*, vol. 116, no. 31, Article ID 104059, 2021.

[9] W. H. Xiao, H. T. Yu, Y. Yuan, L. Taerwe, and R. Chai, "Compression–bending behavior of a scaled immersion joint," *Tunnelling and Underground Space Technology*, vol. 49, pp. 426–437, 2015.

[10] Z. N. Hu and Y. L. Xie, "Mechanical and failure characteristics of shear keys on immersed tunnel segment joints under differential settlements," *Procedia Engineering*, vol. 166, pp. 373–378, 2016.

[11] X. B. Huang, X. Q. Xu, J. H. Luo, and Y. Haitao, "Mechanical performance simulation of immersed tunnel joint under compression-torsion-shear combined loads," *Tunnel Construction*, vol. 37, no. 3, pp. 307–314, 2017.

[12] B. Deng, Z. Niu, and Q. H. Wu, "Study on layout scheme of sliding rails for immersed tunnel section prefabrication plant," *Applied Mechanics and Materials*, vol. 501-504, pp. 1672–1677, 2014.

[13] X. D. Li, Y. R. Zheng, Y. Yuan, and J. X. Wang, "Strength reduction method for submarine immersed tunnels," *Chinese Journal of Geotechnical Engineering*, vol. 35, no. 10, pp. 1876–1882, 2013.

[14] L. Zhu, W. Q. Ding, R. Wang et al., "Analysis of equivalent coefficient of subgrade reaction considering variability of layered soils," *Chinese Journal of Rock Mechanics and Engineering*, vol. 33, no. S1, pp. 3036–3041, 2014.

[15] Z. N. Hu, Y. L. Xie, H. G. Zhang, and X. B. Yue, "Structure reasonableness of segmental joint shear keys on immersed tunnel," *Journal of Chang'an University (Natural Science Edition)*, vol. 35, no. 6, pp. 103–109, 2015.

[16] Z. N. Hu, H. G. Zhang, Y. L. Xie, and X. Yue, "The design and application of a large-scale model test for a super-long immersed tunnel," *Modern Tunnelling Technology*, vol. 51, no. 6, pp. 123–128, 2014.

[17] Y. Yuan, H. T. Yu, W. H. Xiao, and G. P. Xu, "Experimental failure analysis on concrete shear keys in immersion joint subjected to comperssion-shear loading," *Engineering Mechanics*, vol. 34, no. 3, pp. 149–154, 2017.

[18] Z. Zhou, J. J. Zhang, and C. J. Gong, "Automatic detection method of tunnel lining multi-defects via an enhanced You Only Look once network," *Computer-Aided Civil and Infrastructure Engineering*, vol. 37, no. 6, pp. 762–780, 2022.

[19] W. Lin, M. Lin, X. D. Liu, H. Yin, and J. Gao, "Novelties in the islands and tunnel project of the Hong Kong–Zhuhai–Macao Bridge," *Tunnelling and Underground Space Technology*, vol. 120, Article ID 104287, 2022.